Superlattice barrier HgCdTe nBn infrared photodetectors: validation of the effective mass approximation

N. D. Akhavan, G. A. Umana-Membreno, R. Gu, M. Asadnia, J. Antoszewski and L. Faraone

***Abstract*—Implementation of the unipolar barrier detector concept in HgCdTe-based compound semiconductor alloys is a challenging problem, primarily because practical lattice-matched materials that can be employed as the wide bandgap barrier layer in HgCdTe nBn structures present a significant valence band offset at the n-type/barrier interface, thus impeding the free flow of photogenerated minority carriers. However, it is possible to minimise the valence band offset by replacing the bulk HgCdTe alloy-based barrier with a CdTe-HgTe superlattice barrier structure. In this paper, an 8×8 k.p Hamiltonian combined with the non-equilibrium Green's function formalism, has been employed to numerically demonstrate that the single-band effective mass approximation is an adequate numerical approach which is valid for the modelling, design, and optimisation of band alignment and carrier transport in HgCdTe-based nBn detectors incorporating a wide bandgap superlattice barrier.**

***Index Terms* – mercury cadmium telluride (HgCdTe), unipolar barrier, nBn detector, infrared , 8×8 k.p, numerical simulation, non-equilibrium Green's function (NEGF)**

I. INTRODUCTION

The family of unipolar barrier nBn infrared (IR) photodetectors based on the n (contact) B (barrier) n (absorber) structure represent a new device concept compared to conventional photovoltaic technology, and have demonstrated improved performance at higher operating temperatures [2, 3]. In particular, detectors based on the nBn concept utilizing III-V compound semiconductor technology have demonstrated a significant increase in operating temperature from the typical 77K to around 150K; however, implementation of the nBn detector concept in the HgCdTe compound semiconductor system is not straightforward [4-10]. This is due to the fact that the heterointerfaces present in the HgCdTe nBn detector, when formed employing $Hg_{1-x}Cd_xTe$ alloys, exhibit a type-III heterostructure band alignment that results in a relatively large valence band offset at the barrier/n-type absorber hetero interface, thus significantly blocking the flow of photogenerated minority carriers from the absorber layer to the contact layer [7-12]. As illustrated in Fig. 1, this relatively large valence band offset (ΔE_V) severely degrades the performance of HgCdTe-based nBn detectors in comparison to the ideal unipolar nBn detector in which a negligible ΔE_V is present at the barrier/n-type absorber heterointerface.

The authors are with the School of Electrical, Electronic and Computer Engineering, The University of Western Australia, Crawley, 6009, WA. (email: nima.dehdashti@uwa.edu.au)

The authors wish to acknowledge Australian Research Council (ARC) for financial support of this work under the Discovery Project program (grants DP120104835, DP140103667, DP140103667, and DP150104839), the Australian National Fabrication Facility (ANFF) and the Office of Science of the State Government of Western Australia.

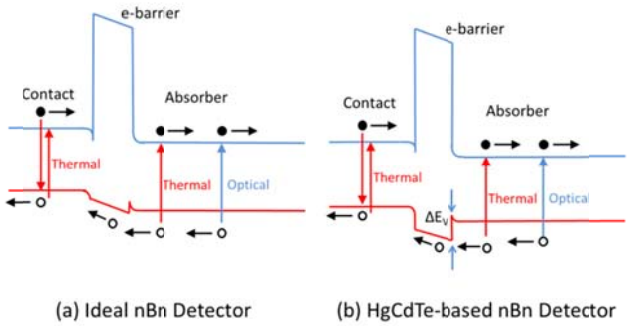

Fig. 1. (a) Ideal unipolar nBn photodetector with negligible valence band offset (ΔE_V), and (b) HgCdTe-based nBn detector with barrier layer exhibiting a relatively large ΔE_V, in which the flow of photogenerated minority carriers in the absorber to the contact layer is affected by ΔE_V.

Several bandgap engineering approaches have been proposed to minimize ΔE_V to values below or approaching the thermal energy of minority carriers [10, 11, 13, 14]. These designs propose lowering ΔE_V at the barrier/n-type heterointerface by grading both the doping and composition across the interface formed employing HgCdTe alloys or, alternatively, propose the use of superlattice-based barrier structures. Of these two bandgap engineering approaches, the superlattice method is the most promising since it does not demand the need for highly controlled graded p-type doping in the barrier layer, which can be problematic in HgCdTe [11]. It is noted, however, that superlattices have yet to be studied in detail as suitable barrier layers for nBn photodetector designs. In their report, Kopytko and co-workers modelled superlattice-barrier HgCdTe nBn detectors employing a simple Kronig-Penny model, and the solution to the eigenvalue problem, in order to calculate the equilibrium energy levels in a CdTe-HgTe-CdTe quantum-well structure. The obtained energy levels were then used to approximate an equivalent effective-mass, bandgap and band alignment, which were then employed in an effective-mass commercial solver to predict the dark current and photogenerated current of a superlattice-

barrier HgCdTe detector [11]. While this device modelling method is convenient and relatively easy to implement, it does not adequately capture the fundamental physical details associated with the superlattice structure, such as wavefunction overlap, density of states, nor the influence of layer doping on the resulting band diagram. In this work, we present results of a full quantum mechanical approach based on the non-equilibrium Green's function (NEGF) to predict the carrier transmission and band diagram of the HgCdTe nBn detector with superlattice barrier [15, 16]. Bulk 8×8 k.p Hamiltonian parameters for HgTe and CdTe have been employed to calculate the electronic structure. Although the 8×8 k.p calculations employed for modelling are more computationally intensive than a simple one-band effective mass approximation, our results indicate that the latter approach yields accurate results which can also be used to model the band structure and carrier transport in HgCdTe nBn structures, and to predict the performance of nBn infrared photodetectors [16-18].

II. NUMERICAL SIMULATION DETAILS

The electronic properties of a superlattice barrier nBn HgCdTe detector structure are determined by the electronic properties of the individual layers that form the superlattice basis. From a semiconductor growth technology viewpoint, the simplest superlattice basis structure in the HgCdTe alloy system is to employ the binary compounds HgTe and CdTe. However, it is noted that, in practice, the high Hg over-pressure during molecular beam epitaxial growth of HgCdTe is likely to result in a superlattice structure comprised of HgTe and a high x-value $Hg_{0.05}Cd_{0.95}Te$ alloy. Thus, the starting point is the band structure calculation for a CdTe/HgTe/CdTe basis structure of the superlattice, in which the band structure parameters for the superlattice defined by the 8-band k.p Hamiltonian at T=0 K are summarized in Table 1. It should be noted that superlattice electronic properties have been theoretically analysed employing several approaches, including tight binding, pseudopotentials, and density functional theory, in addition to 8×8 k.p. However, the k.p envelope function approach has been shown to yield results that are similar to other approaches [1, 19]. In addition, the k.p method is particularly valid around the gamma point of the band structure where, the relevant physics of an nBn detector are determined. More importantly, and in contrast to the parameters required for other theoretical approaches, the band structure parameters for CdTe and HgTe materials are well established in the k.p framework [1, 20]. Details of the 8×8 k.p Hamiltonian and the numerical discretization is provided in the Appendix.

Table 1. Band structure parameters of HgTe and CdTe. E_g is the energy gap, Δ is the spin-orbit splitting energy, Λ is the valence band offset between the two materials, E_P is the energy related to the Kane momentum matrix element P, F is related to the normalized conduction band effective mass m_c/m_0, and γ_i's are the valence band Luttinger parameters [1].

Band parameter	HgTe	CdTe
E_g (eV)	-0.303	1.606
Δ (eV)	1.08	0.91
Λ (eV)	0	0.350
E_P (eV)	18.8	18.8
F	0	-0.09
γ_1	4.1	1.47
γ_2	0.5	-0.28
γ_3	1.3	0.03

Following the method in the Appendix, and setting up the discretized Hamiltonian, the band structure of the bulk material is calculated by solving:

$$\left(D_i + D_i^+ e^{+ik_z} + D_{i+1}^- e^{-ik_z}\right)\psi_i = E_i \psi_i \tag{1}$$

where k_z is the wavenumber in the transport direction, and E_i, ψ_i are the eigenvalue and eigenfunction of layer i, respectively. For the simplest case of a bulk material band structure, since there is only one material type which does not vary along the transport direction z, the matrix D takes the form:

$$\begin{aligned} D_{i-1} &= D_i = D_{i+1} \\ D_{i-1}^+ &= D_i^+ = D_{i+1}^+ \\ D_{i-1}^- &= D_i^- = D_{i+1}^- \end{aligned} \tag{2}$$

and hence, the band structure of bulk material can be calculated by setting i=0, which gives,

$$\left(D_0 + D_0^+ e^{+ik_z} + D_0^- e^{-ik_z}\right)\psi_0 = E_0 \psi_0 \tag{3}$$

The band structure of bulk CdTe and HgTe thus calculated is presented in Fig. 2, where it can be seen that CdTe exhibits a normal direct band gap structure, with the conduction band minimum (Γ_6) located above the valence band maximum (Γ_8). In contrast, HgTe manifests an inverted band structure in which hole states (Γ_8) are located above the electron states (Γ_6). It is also possible to extract the effective mass of electrons, heavy holes and light holes from the bulk band structures. The effective mass at the Γ point is equal to the inverse of the $E(k)$ curvature at k=0, which is given by,

$$m^* = \frac{\hbar^2}{q m_0}\left(\left.\frac{d^2 E(k)}{dk^2}\right|_{k=0}\right)^{-1} \tag{4}$$

where m_0 and $\hbar$ are the free electron rest mass and the reduced Planck constant, respectively. The band structure of CdTe and HgTe calculated using the 8×8 k.p Hamiltonian and the equivalent parabolic band approximation using the effective masses of Γ_6 and Γ_8 bands for electrons and heavy holes are shown in Fig. 2. From the k.p calculations, the effective mass of electrons in the Γ_6 band is equal to 0.031 and 0.090 for HgTe and CdTe, respectively, whereas the effective mass of heavy holes in the Γ_8 band is equal to 0.3226 and 0.4926 for HgTe and CdTe, respectively. These values of effective mass are in good agreement with reported values by other groups, thus validating our approach [19, 21].

Having detailed the methodology to construct the Hamiltonian for both bulk material and superlattice structures, and verified that the parabolic effective mass approximation yields band structure results consistent with the 8-band k.p in

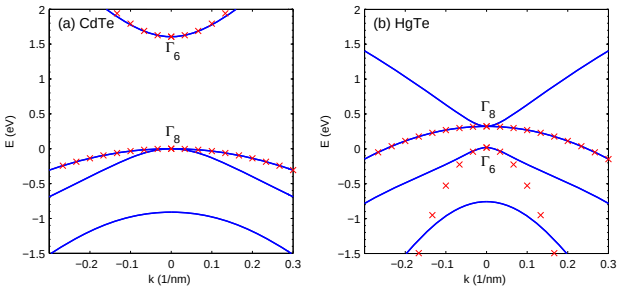

Fig. 2. Bulk band structure (solid lines) of (a) CdTe and, (b) HgTe from the 8×8 k.p calculations. The relative position of the conduction band minimum and valence band maximum at the minimum bandgap at k=0 in HgTe is opposite to that in CdTe; in HgTe, the Γ_8 hole states lie above the Γ_6 electron states. Also shown by the (×) symbols are the corresponding parabolic energy dispersion band structure characteristics calculated using the effective mass approximation for conduction band electrons and valence band heavy holes. The effective mass approximation adequately describes the band structure of electrons and heavy holes close to the Γ point at k=0.

bulk HgCdTe materials, we can proceed to calculate the band structure of the HgTe/CdTe superlattice barrier basis using the quantum well (QW) "building block" shown schematically in Fig. 3. Thus, the QW is taken as the unit cell in a periodic one-dimensional superlattice in the growth direction z by imposing periodic boundary conditions, which is a reasonable approximation to describe the physics of quantum transport near the Γ point. In Fig. 3, D_{QW} represents the discretized Hamiltonian matrix of the QW unit cell in the z direction, and D_U corresponds to the matrix connecting adjacent unit cells. The D_{QW} matrix is effectively equivalent to D_i, in (2), and is thus constructed exactly in the same way. The final form of the complete Hamiltonian matrix for periodically arranged QWs in the superlattice structure is given by:

$$H_{QW} = \begin{pmatrix} & & \cdots & & \\ D_L & D_{QW} & D_U & & \\ & D_L & D_{QW} & D_U & \\ & & D_L & D_{QW} & D_U \\ & & \cdots & & \end{pmatrix} \tag{5}$$

with,

$$D_U = \begin{pmatrix} 0 & & & 0 \\ \cdots & & \iddots & \\ 0 & 0 & & \\ D_{N_x}^{+} & 0 & \cdots & 0 \end{pmatrix} \tag{6}$$

$$D_L = \begin{pmatrix} 0 & \cdots & 0 & D_{N_x}^{-} \\ & & & 0 \\ & \iddots & & \vdots \\ 0 & & & 0 \end{pmatrix} \tag{7}$$

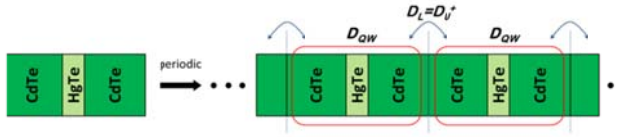

Fig. 3. Schematic representation of the HgTe/CdTe quantum well "building block" and its corresponding periodic superlattice structure. D_L and D_U are matrices which link two adjacent cells.

where D_{QW}, D_L and D_U are all of size $(N_z \times N_b)\times(N_z \times N_b)$, and N_b is the number of bands (N_b=8 for the 8-band k.p Hamiltonian, or N_b=1 for the single-band effective mass Hamiltonian). D_L and D_U are matrices that serve to link two adjacent QW unit cells in the periodic representation. The band structure of the QW superlattice is then calculated from:

$$\left(D_{QW} + D_U e^{+ik_z} + D_L e^{-ik_z}\right)\psi = E\psi \tag{8}$$

The above equations allow calculation of the superlattice band structure which, in the most general case, demands the calculation of eigenvalues using the relatively large matrices of D_{QW}, D_L and D_U over k_z values of interest. For the simplest and most relevant case of k_z in the vicinity of the Γ point, however, setting k_z=0 reduces the computational cost while allowing the calculation of available energy levels within the superlattice structure in the framework of the parabolic band effective mass approximation.

III. RESULTS AND DISCUSSION

The energy levels calculated for a 2nm/8nm HgTe/CdTe quantum well basis, obtained employing the above detailed 8×8 k.p theoretical simulation framework, are presented in Fig. 4 in relation to their energy location within the band diagram as well as their energy-momentum dispersion. The CdTe and HgTe layer thicknesses were chosen within a specific range (i.e. 1nm<HgTe<3nm and 5nm<CdTe<8nm) in order to achieve an equivalent barrier bandgap that is significantly larger than the bandgap of the absorber region in an nBn structure [11]. It is evident that the eigenvalues of the quantum well match the energy levels of the E-k dispersion diagram at k=0.

The energy levels for the HgTe/CdTe superlattice as a function of HgTe layer width were then calculated both employing the 8-band k.p Hamiltonian and the single-band effective mass approximation. The calculated results presented in Fig. 5 clearly indicate that as the thickness of the HgTe layer increases, the conduction band electron energy levels predicted by the one band effective mass approximation deviate from those obtained from the more rigorous 8-band k.p approach [22]. This is a consequence of increased band mixing arising from the influence of remote bands, an effect that is neglected in the one-band effective mass approximation. Since the electron mass is much lighter than the heavy hole mass in the valence band, this effect is more readily evident on the electron states in the conduction band.

The energy levels of the HgTe/CdTe superlattice were calculated without taking into account that, in practical nBn detector structures, the HgTe/CdTe superlattice is constrained to have a finite number of QW building blocks and is bounded

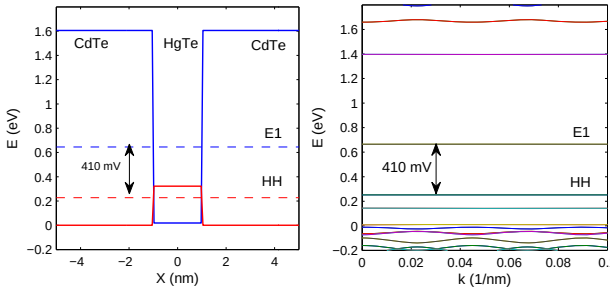

Fig. 4. (left) Energy levels of HgTe/CdTe quantum well unit cell, with a HgTe layer thickness of 2nm, calculated using the 8×8 k.p Hamiltonian, and (right) band structure of the quantum well with $\boldsymbol{k}_{\|}$ (k_y=0, k_x=0).

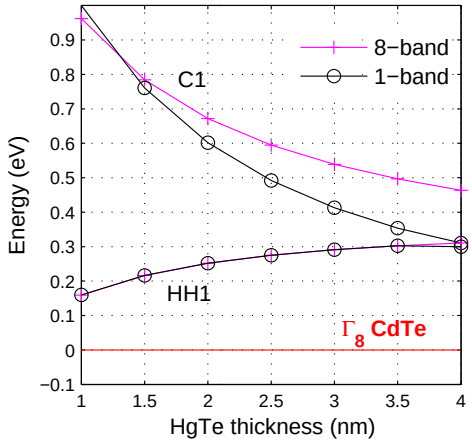

Fig. 5. Energy levels of HgTe/CdTe quantum well as a function of HgTe layer thickness for a fixed CdTe thickness of 8nm, calculated using the 8×8 k.p Hamiltonian and equivalent one-band effective mass approximation at the Γ point with $\boldsymbol{k}_{\|}$ (k_y=0, k_x=0) and k_z=0.

on both sides by adjacent narrow gap absorber and contact regions. For the practical design of a superlattice-barrier nBn detector a more sophisticated approach, such as the density matrix theory, transfer matrix method (TMM) or the non-equilibrium Green's function (NEGF) formalism, is required in order to gain better insight into the available energy states participating in carrier transport across the superlattice barrier region [16-18, 23, 24]. In particular, these methods take into account effects associated with density of states, wavefunction overlap, charge density, scattering mechanisms, and tunnelling phenomenon. In what follows, we employ the NEGF approach, which has been proven to be a powerful approach for the calculation of electronic properties and carrier transport in semiconductor devices where quantum effects are dominant [24].

NEGF modelling approach

In contrast to the periodic arrangement required to calculate the energy levels of the superlattice alone, which correspond to the effective bandgap presented by the superlattice as a barrier in nBn photodetector structures, the NEGF approach enables theoretical calculation of energy states and carrier transport probabilities using the actual layered structure of an nBn device, as depicted in Fig. 6. The absorber and contact regions are composed of bulk $Hg_{0.3}Cd_{0.7}Te$ material, and thus

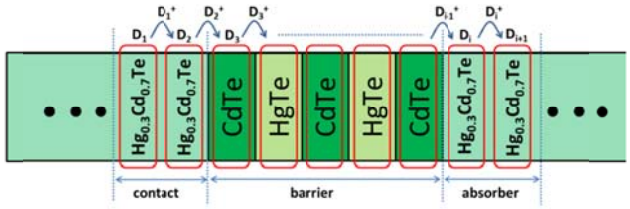

Fig. 6. Schematic representation of HgCdTe nBn detector with superlattice barrier treated as a layered structure.

corresponds to an nBn structure optimised for detection of midwave IR (3-5 µm wavelength band). As detailed previously, the diagonal blocks of the Hamiltonian matrix D represent the interaction within each layer of the detector, whereas the off-diagonal blocks of matrix D couple adjacent layers (denoted $D_i^+=D_{i+1}^-$), thus ensuring that D is Hermitian. The NEGF equation for quantum transport can then be expressed as [25]:

$$G(E)=\left[(E+i\eta)I-D-\Sigma_L(E)-\Sigma_R(E)\right]^{-1} \tag{9}$$

where G is the Green's function, Σ_L and Σ_R are the self-energy matrices, E is the energy, and η is an infinitesimally small number. Since the Hamiltonian D is infinite at the left and right extremities of a realistic nBn detector structure, we adopt the self-energy matrix concept to render it finite, which can be calculated using recursive methods such as the Sancho-Rubio algorithm or direct methods which are based on solving the eigenvalue problem [26]. In this study we have used a recursive algorithm implementation, an in-house developed software which is based on the previous works [24,25].

Following calculation of the Green's function for the practical detector structure, the transmission probability for carrier injection across the barrier at different energies is calculated from [25]:

$$T(E)=trace\left(G(E)\Gamma_L(E)G^+(E)\Gamma_R(E)\right) \tag{10}$$

$$\Gamma_L=i\left(\Sigma_L-\Sigma_L^+\right) \tag{11}$$

$$\Gamma_R=i\left(\Sigma_R-\Sigma_R^+\right) \tag{12}$$

where T is the transmission probability, Γ_L and Γ_R are broadening matrices, and "*trace*" is the summation over all diagonal elements of the matrix. The matrix G is a retarded Green's function matrix, with the imaginary component of the diagonal elements corresponding to the local density of states (LDOS). The calculated local density of states, transmission probabilities, and eigenenergies for a HgCdTe nBn detector structure and, with 1 nm HgTe and 1 nm CdTe layer thicknesses, a total superlattice barrier thickness of 5 nm are presented in Fig. 7. It is evident that the carrier transmission probability peaks at energy levels corresponding to the highest local density of states located at ~0.8 eV and ~1eV. It should be noted that while the energies obtained from solution of the eigenvalue problem align with energy locations where the maximum LDOS occur, a solution of the eigenvalue problem cannot predict the overlap of the wavefunctions from adjacent wells and is thus unable to model the transmission probability broadening that determines the flow of carriers across the superlattice barrier.

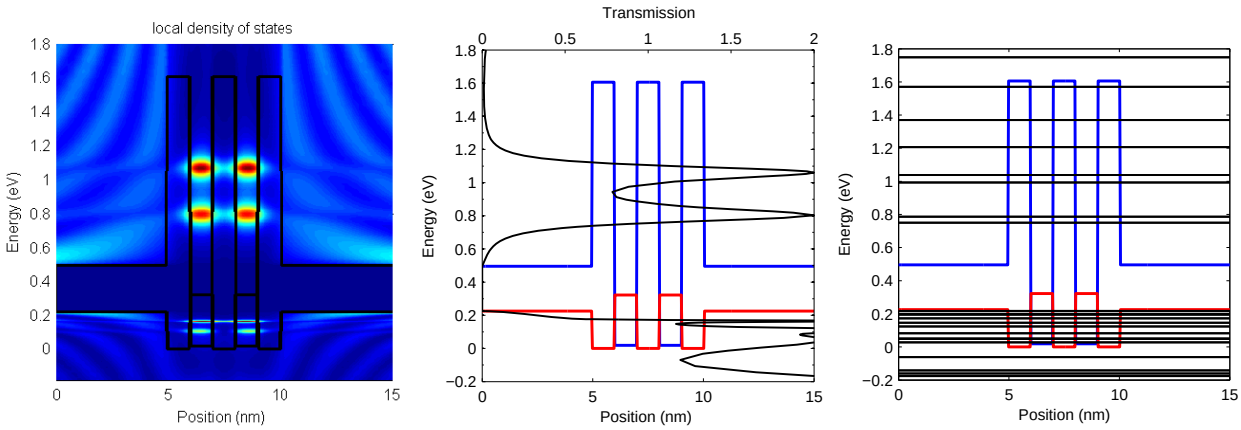

Fig. 7. From left to right: LDOS, transmission probability, and eigenvalues of HgCdTe nBn detector calculated using the 8×8 k.p Hamiltonian. The superlattice layers have a barrier width of 1nm and a well width of 1nm. The peaks in the transmission probability correspond to energy levels where the LDOS is maximum, which represent energy levels at which carrier transport across the barrier can take place.

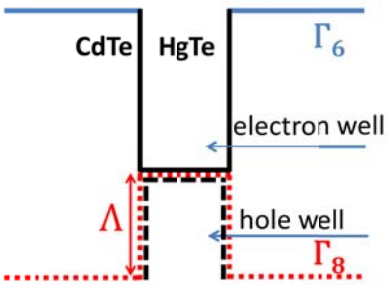

Fig. 8. Schematic diagram of energy band alignment in the HgTe-CdTe system used in [11]. Λ represents the valence band offset. The superlattice electron and heavy-hole states are associated with the quantum well for electrons (thick solid black line) and the quantum well for heavy holes (thick dashed black line).

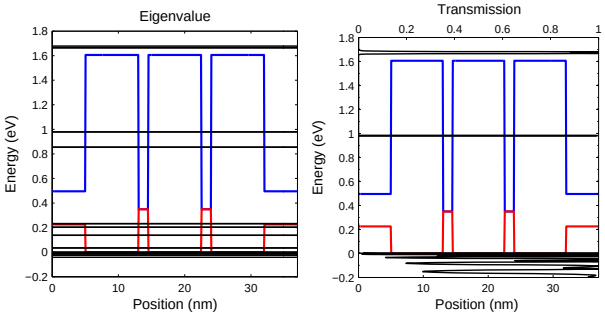

Fig. 9. Comparison of resonance states calculated from (left) an eigenvalue solver, and (right) the NEGF solver using the single-band effective mass approximation. The CdTe-HgTe thicknesses are 8 nm and 1.5 nm, respectively.

Recently, Kopytco *et. al.* determined the energy levels of a CdTe/HgTe superlattice as a function of well width [11]. The schematic diagram of the quantum well is shown in Fig. 8. In this diagram, the bottom of the electron well and top of the heavy-hole well are located at the same energy level relative to the CdTe valence band edge Γ_8, and has a value determined by the valence band offset Λ=350 meV. The effective mass values used for each layer are the same as those used by Kopytco *et. al.* [11]. Fig. 9 compares the resonance levels calculated from an eigenvalue solver (left) and the NEGF solver (right). Of particular relevance, are the resonance states above the conduction band edge of the bulk HgCdTe material, which is at 0.5 eV. It can be observed that the eigenvalue solver predicts two resonance states in the barrier conduction band, whereas the transmission probability from the NEGF solver indicates that only one of these states is available for carrier transport. A similar situation exist for valence band resonance states, where the eigenvalue solver predicts many states; whereas the transmission probability obtained from the NEGF approach indicates that only those resonance states below 0 eV can contribute to carrier transport. Fig. 10 shows the calculated resonance states of the superlattice as a function of HgTe thickness for a fixed CdTe thickness of 8 nm, where the resonance levels predicted by Kopytco *et. al.* have been compared with our NEGF and eigenvalue solver. In this figure the two lowest energy levels in the conduction band have been plotted and labelled as eig-1 and eig-2. It is evident that for HgTe thickness less than 2nm, the second eigenvalue is in agreement with the transmission probability from our NEGF and with the results of Kopytco *et. al.*. For the hole resonance states, our eigenvalue results match with the results of Kopytco *et. al.*, which have not been plotted for clarity. However, note that the hole transmission probabilities calculated from our NEGF results indicate that the hole states with energies above 0 eV do not contribute to carrier transport.

It is now appropriate to compare results from the 8×8 k.p Hamiltonian calculations with those from a single-band effective mass approximation for the nBn superlattice device. Fig. 11 shows the schematic band diagram of the CdTe/HgTe quantum well associated with the superlattice, where the bottom of the electron quantum well is located at the Γ_6 band edge of the HgTe, and the top of the hole quantum well is located at the Γ_8 band edge of the HgTe. It should be noted that this is different from the electron/hole quantum well definition used by Kopytco *et. al.*[11]. Fig.12 shows the eigenvalues of an nBn superlattice device calculated using the 8×8 k.p Hamiltonian and the single-band effective mass approximation. Compared to the effective mass approximation, there are several eigenvalues from the k.p calculations that arise from band mixing of heavy-holes and electrons; however, only the eigenvalue located at 0.75 meV is shared between the k.p and effective mass calculations. Fig. 13

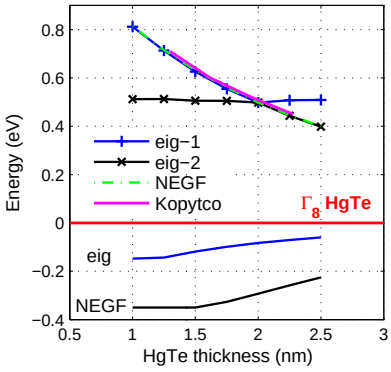

Fig. 10. Electron and heavy-hole resonance states as a function of the thickness of the HgTe layer for a fixed CdTe thickness of 8 nm, calculated using the single-band effective mass Hamiltonian. The lines above and below Γ_8 corresponds to electrons and holes, respectively.

shows the transmission probability of carriers through the barrier calculated using the NEGF formalism in the same nBn superlattice for an 8×8 k.p Hamiltonian and a single-band effective mass approximation. It is clear that despite having several eigenvalues (as indicated in Fig. 12), only certain energy levels contribute to carrier transport through the barrier, which depend on the carrier wavefunction overlap and density of states. It is evident that both the 8×8 k.p and single-band effective mass calculations show the same transmission probability for electrons, whereas in the case of holes the single-band effective mass indicates a different transmission probability compared to the 8×8 k.p approach, which is due to the complicated band mixing that is taken into account by the 8×8 k.p model. Fig. 14 shows the electron and heavy-hole energy levels as a function of HgTe well width calculated via the NEGF formalism for the case of an 8-band and a single-band Hamiltonian. It is clear that the electron states predicted by the single-band approximation are in a good agreement with those obtained from the 8×8 k.p Hamiltonian, whereas the heavy-hole states strongly depend on band-mixing and well width. However, for the specific nBn detectors in this paper, we noticed that choosing the heavy-hole effective mass equal to 0.15 can lead to hole states which are in good agreement with those predicted by an 8×8 k.p Hamiltonian, as shown in Fig. 14b.

IV. CONCLUSIONS

We have performed a theoretical study of band structure and quantum carrier transport in superlattice barrier HgCdTe nBn detector structures using a full quantum mechanical approach using the NEGF formalism. The presented results indicate that the HgTe layer thickness in a HgTe/CdTe superlattice barrier has a strong effect on the band alignment between the absorber and barrier, indicating that it needs to be critically controlled in order to simultaneously obtain a large conduction band offset and a minimum valence band offset. Our results indicate that for quantum-well structures with a well width of less than 2 nm, a single-band effective mass approximation, when coupled with the NEGF approach, yields results that are in relatively good agreement with those obtained employing the

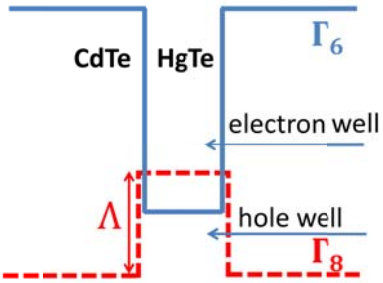

Fig. 11. Schematic diagram of energy band alignment in the HgTe-CdTe system used in this paper, in which Λ is the valence band offset. The superlattice electron and heavy-hole states are associated with the quantum well for electrons (solid line) and the quantum well for heavy holes (dotted line).

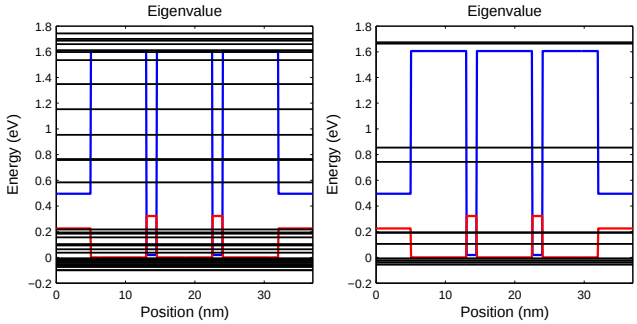

Fig. 12. Calculated eigenvalues from (left) 8-band k.p model, and (right) a single-band effective mass model. In this configuration, the CdTe thickness is 8 nm and HgTe thickness is 1.5nm.

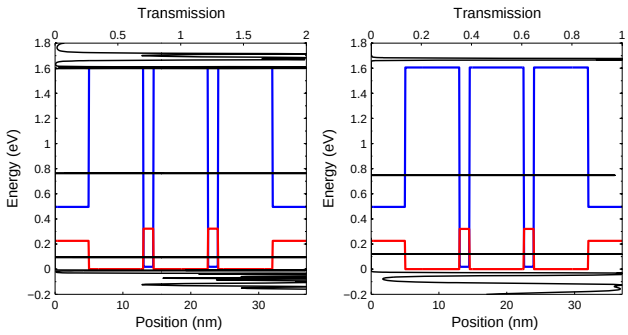

Fig. 13. Carrier transmission probability calculated using the NEGF formalism, (left) an 8-band k.p model, and (right) a single-band effective mass model. In this configuration, the CdTe thickness is 8 nm and the HgTe thickness is 1.5nm.

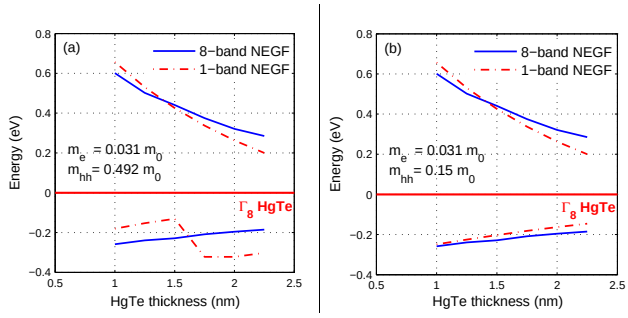

Fig. 14. Comparison of electron states and heave-hole states as a function of well width calculated using the NEGF formalism for an 8-band Hamiltonian and a single-band Hamiltonian. In this configuration, CdTe thickness is fixed at 8 nm. (a) single-band with heavy-hole effective mass fitted to 8-band k.p band structure, and (b) empirical energies using a fixed heavy-hole effective mass of 0.15 to obtain a better agreement with k.p approach.

more computationally intensive 8×8 k.p Hamiltonian in NEGF based calculations.

APPENDIX

In order to construct the superlattice nBn detector Hamiltonian, we start with the 8-band k.p envelope function Hamiltonian defined in the (001) growth direction, which is a well-accepted model and has been previously used by several groups to calculate the band structure of HgTe/CdTe in bulk, quantum well, and superlattice configurations [1, 27]. Therefore, assuming $\boldsymbol{k}_{\parallel}=k_x^2+k_y^2$ and $\boldsymbol{k}\equiv(\boldsymbol{k}_{\parallel},k_z)=(0,0,k_z)$, the full 8×8 k.p Hamiltonian reduces to:

$$H(k_{\parallel}=0,k_z)=$$

$$\begin{pmatrix} \varepsilon_c & 0 & 0 & \hbar k_z t & 0 & 0 & \frac{-\hbar k_z t}{\sqrt{2}} & 0 \\ 0 & \varepsilon_c & 0 & 0 & \hbar k_z t & 0 & 0 & \frac{\hbar k_z t}{\sqrt{2}} \\ 0 & 0 & \varepsilon_H & 0 & 0 & 0 & 0 & 0 \\ \hbar k_z t & 0 & 0 & \varepsilon_L & 0 & 0 & -\varepsilon_{vs} & 0 \\ 0 & \hbar k_z t & 0 & 0 & \varepsilon_L & & 0 & -\varepsilon_{vs} \\ 0 & 0 & 0 & 0 & 0 & \varepsilon_H & & 0 \\ \frac{-\hbar k_z t}{\sqrt{2}} & 0 & 0 & -\varepsilon_{vs} & 0 & 0 & \varepsilon_s & 0 \\ 0 & \frac{\hbar k_z t}{\sqrt{2}} & 0 & 0 & -\varepsilon_{vs} & 0 & 0 & \varepsilon_s \end{pmatrix} \quad \text{(A1)}$$

with the matrix elements defined by:

$$\varepsilon_c = E_C(z)+\frac{\hbar^2}{2m_0}\left(k_z(2F+1)k_z\right)$$

$$\varepsilon_L = E_V(z)-\frac{\hbar^2}{2m_0}\left(k_z(\gamma_1-2\gamma_2)k_z\right)$$

$$\varepsilon_H = E_V(z)-\frac{\hbar^2}{2m_0}\left(k_z(\gamma_1+2\gamma_2)k_z\right)$$

$$\varepsilon_s = -\Delta(z)-\frac{\hbar^2}{2m_0}\left(k_z(\gamma_1)k_z\right)$$

$$\varepsilon_{vs} = \frac{\sqrt{8}\hbar^2}{2m_0}\left(k_z(\gamma_2)k_z\right)$$

$$t=\sqrt{\frac{E_P}{3m_0}}$$

where E_g is the energy gap, Δ is the spin-orbit splitting energy, Λ is the valence band offset between the two materials, E_P is the energy related to the Kane momentum matrix element P, F is related to the normalized conduction band effective mass m_c/m_0, and γ_i's are the valence band Luttinger parameters.

Discretization

Having identified the Hamiltonian, it needs to be discretized in the growth direction, since this is the direction of carrier transport (i.e. z direction), by replacing the scalar k_z with the differential $k_z \rightarrow -i\partial/\partial z$, and keeping k_x and k_y constant. Using the finite difference method (FDM), the discrete first and second derivatives of the wavefunction can be written as [24, 25]:

$$\frac{\partial\psi}{\partial z}=\frac{\partial\psi_{i+1}-\partial\psi_{i-1}}{2\Delta z} \quad \text{(A2)}$$

$$\frac{\partial^2\psi}{\partial z^2}=\frac{\partial\psi_{i-1}-2\partial\psi_i+\partial\psi_{i+1}}{\Delta z^2} \quad \text{(A3)}$$

where i are the cartesian mesh indices in the z direction, and Δz is the mesh spacing. Correspondingly, for the case of a one dimensional device topology, the discretized Hamiltonian of (A1) can be divided into three matrices, as follows [24]:

$$H(K_{\parallel},kz)=H^{(0)}(K_{\parallel})+H^{(1)}(K_{\parallel})k_z+H^{(2)}(K_{\parallel})k_z^2 \quad \text{(A4)}$$

where $\boldsymbol{k}_{\parallel}=(k_y, k_x)$, and $H^{(i)}$ with $i = 0, 1, 2$ are the 8×8 matrices obtained by writing the k·p Hamiltonian in increasing order of k_z . For example,

$$H^{(1)}(K_{\parallel})=\begin{pmatrix} 0 & 0 & 0 & \hbar t & 0 & 0 & \frac{-\hbar t}{\sqrt{2}} & 0 \\ 0 & 0 & 0 & 0 & \hbar t & 0 & 0 & \frac{\hbar t}{\sqrt{2}} \\ 0 & 0 & 0 & 0 & 0 & 0 & 0 & 0 \\ cc & 0 & 0 & 0 & 0 & 0 & 0 & 0 \\ 0 & cc & 0 & 0 & 0 & 0 & 0 & 0 \\ 0 & 0 & 0 & 0 & 0 & 0 & 0 & 0 \\ cc & 0 & 0 & 0 & 0 & 0 & 0 & 0 \\ 0 & cc & 0 & & 0 & 0 & 0 & 0 \end{pmatrix} \quad \text{(A5)}$$

where cc is the complex conjugate of the corresponding upper diagonal matrix element. Thus, the discretized equations at all grid points can be expressed as a single block tri-diagonal matrix D as follows:

$$D=\begin{pmatrix} & & \cdots & & \\ D_{i-1}^- & D_{i-1} & D_{i-1}^+ & & \\ & D_i^- & D_i & D_i^+ & \\ & & D_{i+1}^- & D_{i+1} & D_{i+1}^+ \\ & & \cdots & & \end{pmatrix} \quad \text{(A6)}$$

where,

$$D_i=+\frac{2H_i^{(2)}+H_{i-1}^{(2)}+H_{i+1}^{(2)}}{2\Delta z^2}+\frac{2H_i^{(0)}+H_{i-1}^{(0)}+H_{i+1}^{(0)}}{4} \quad \text{(A7)}$$

$$D_i^-=-\frac{H_i^{(2)}+H_{i-1}^{(2)}}{2\Delta z^2}+i\frac{H_i^{(1)}+H_{i-1}^{(1)}}{4\Delta z} \quad \text{(A8)}$$

$$D_i^+=-\frac{H_i^{(2)}+H_{i+1}^{(2)}}{2\Delta z^2}-i\frac{H_i^{(1)}+H_{i+1}^{(1)}}{4\Delta z} \quad \text{(A9)}$$

Thus, the complete detector matrix D, defined by (A6), has a size of $(N_z\times N_b)\times(N_z\times N_b)$, where N_z defines the number of grid points in the z-direction, and N_b is the number of bands in the Hamiltonian matrix of the material (in our case N_b=8, but it can be any number). The above matrix definition is valid for

bulk structures as well as quantum-wells, superlattices, and heterostructures, where the material parameters change between adjacent grid points i and i+1 in the growth direction. It is also valid for any type of Hamiltonian, whether it is single-band or multi-band. As mentioned earlier, the parameters summarized in Table 1 correspond to the (001) growth direction, whereas all the equations are valid for any crystal orientation. The H matrix in (A1) can be transformed to any desired growth direction by applying an appropriate "transformation matrix", as detailed in reference [24].

REFERERENCES

[1]E. G. Novik, A. Pfeuffer-Jeschke, T. Jungwirth, V. Latussek, C. R. Becker, G. Landwehr, H. Buhmann, and L. W. Molenkamp, "Band structure of semimagnetic $Hg_{1-y}Mn_yTe$ quantum wells," *Physical Review B,* vol. 72, p. 035321, 2005.

[2]S. Maimon and G. W. Wicks, "nBn detector, an infrared detector with reduced dark current and higher operating temperature," *Applied Physics Letters,* vol. 89, p. 151109, 2006.

[3]P. Martyniuk, M. Kopytko, and A. Rogalski, "Barrier infrared detectors," *Opto-Electronics Review,* vol. 22, pp. 127-146, 2014.

[4]N. Gautam, H. S. Kim, M. N. Kutty, E. Plis, L. R. Dawson, and S. Krishna, "Performance improvement of longwave infrared photodetector based on type-II InAs/GaSb superlattices using unipolar current blocking layers," *Applied Physics Letters,* vol. 96, p. 231107, 2010.

[5]B.-M. Nguyen, D. Hoffman, P.-Y. Delaunay, and M. Razeghi, "Dark current suppression in type II InAs⁄GaSb superlattice long wavelength infrared photodiodes with M-structure barrier," *Applied Physics Letters,* vol. 91, pp. -, 2007.

[6]J. B. Rodriguez, E. Plis, G. Bishop, Y. D. Sharma, H. Kim, L. R. Dawson, and S. Krishna, "nBn structure based on InAs⁄GaSb type-II strained layer superlattices," *Applied Physics Letters,* vol. 91, p. 043514, 2007.

[7]N. D. Akhavan, G. Jolley, G. Umana - Membreno, J. Antoszweski, and L. Faraone, "Design Parameters for High-Performance HgCdTe-Based nBn Detectors Structures," in *2013 U.S. Workshop on the PHYSICS and CHEMISTRY of II-VI MATERIALS*, 2013.

[8]N. D. Akhavan, G. Jolley, G. A. Umana-Membreno, J. Antoszewski, and L. Faraone, "Performance Modeling of Bandgap Engineered HgCdTe-Based nBn Infrared Detectors," *IEEE Transactions on Electron Devices,* vol. 61, pp. 3691-3698, 2014.

[9]N. D. Akhavan, G. Jolley, G. A. Umana-Membreno, J. Antoszewski, and L. Faraone, "Design of Band Engineered HgCdTe nBn Detectors for MWIR and LWIR Applications," *IEEE Transactions on Electron Devices,* vol. 62, pp. 722-728, 2015.

[10]N. D. Akhavan, G. A. Umana-Membreno, G. Jolley, J. Antoszewski, and L. Faraone, "A method of removing the valence band discontinuity in HgCdTe-based nBn detectors," *Applied Physics Letters,* vol. 105, p. 121110, 2014.

[11]M. Kopytko, J. Wróbel, K. Jóźwikowski, A. Rogalski, J. Antoszewski, N. D. Akhavan, G. A. Umana-Membreno, L. Faraone, and C. R. Becker, "Engineering the Bandgap of Unipolar HgCdTe-Based nBn Infrared Photodetectors," *Journal of Electronic Materials,* vol. 44, pp. 158-166, 2014.

[12]A. M. Itsuno, J. D. Phillips, and S. Velicu, "Design and Modeling of HgCdTe nBn Detectors," *Journal of Electronic Materials,* vol. 40, pp. 1624-1629, 2011.

[13]J. Antoszewski, N. D. Akhavan, G. Umana-Membreno, R. Gu, W. Lei, and L. Faraone,"Recent Developments in Mercury Cadmium Telluride IR Detector Technology," *ECS Transactions,* vol. 69, pp. 61-75, 2015.

[14]D. Z. Ting, A. Soibel, L. Höglund, C. J. Hill, A. Khoshakhlagh, S. A. Keo, A. M. Fisher, E. M. Luong, J. K. Liu, J. M. Mumolo, S. B. Rafol, S. D. Gunapala, "Carrier transport in unipolar barrier infrared detectors," Proceedings of SPIE, pp. 94510-94510, 2015, DOI: 10.1117/12.2177549

[15]M. Shin, "Quantum transport of holes in 1D, 2D, and 3D devices: the k.p method", *Journal of Computational Electronics,* vol. 10, pp. 44-50, 2011.

[16]U. Aeberhard, "Theory and simulation of photogeneration and transport in Si-$SiO_{(x)}$ superlattice absorbers," *Nanoscale Research Letters,* vol. 6, pp. 242-242, 2011.

[17]N. Cavassilas, F. Michelini, and M. Bescond, "Modeling of nanoscale solar cells: The Green's function formalism," *Journal of Renewable and Sustainable Energy,* vol. 6, p. 011203, 2014.

[18]U. Aeberhard, "Effective microscopic theory of quantum dot superlattice solar cells," *Optical and Quantum Electronics,* vol. 44, pp. 133-140, 2011.

[19]M. Penna, A. Marnetto, F. Bertazzi, E. Bellotti, and M. Goano, "Empirical Pseudopotential and Full-Brillouin-Zone k · p Electronic Structure of CdTe, HgTe, and Hg_{1-x} Cd_xTe," *Journal of Electronic Materials,* vol. 38, pp. 1717-1725, 2009.

[20]J. Benyaya, P. Martyniuk, M. Kopytko, J. Antoszewski, W. Gawron, and P. Madejczyk, "nBn HgCdTe infrared detector with HgTe(HgCdTe)/CdTe SLs barrier," Optical and Quantum Electronics, vol. 48, pp. 1-8, 2016.

[21]C. R. Becker, V. Latussek, A. Pfeuffer-Jeschke, G. Landwehr, and L. W. Molenkamp, "Band structure and its temperature dependence for type-III $HgTe/Hg_{1-x}Cd_xTe$ superlattices and their semimetal constituent," *Physical Review B,* vol. 62, pp. 10353-10363, 2000.

[22]C. H. Grein, H. Jung, R. Singh, and M. E. Flatté, "Comparison of normal and inverted band structure HgTe/CdTe superlattices for very long wavelength infrared detectors," *Journal of Electronic Materials,* vol. 34, pp. 905-908, 2005.

[23]T. M. Abdolkader, "Simulation of Quantum Transport in Ballistic Double-Gate MOSFETs using Transfer Matrix Method," in *2006 International Conference on Computer Engineering and Systems*, 2006, pp. 91-96.

[24]M. Shin, "Quantum transport of holes in 1D, 2D, and 3D devices: the k.p method," *Journal of Computational Electronics,* vol. 10, pp. 44-50, 2009.

[25]S. Datta, "Nanoscale device modeling: the Green's function method," *Superlattices and Microstructures,* vol. 28, pp. 253-278, 2000.

[26]M. P. L. Sancho, J. M. L. Sancho, J. M. L. Sancho, and J. Rubio, "Highly convergent schemes for the calculation of bulk and surface Green functions," *Journal of Physics F: Metal Physics,* vol. 15, p. 851, 1985.

[27]A. Dargys, "Spin properties of $Hg_{1-x}Cd_xTe$/CdTe quantum wells," *physica status solidi (b),* vol. 245, pp. 1483-1492, 2008.

Nima Dehdashti Akhavan (M'08) was born in Tajrish, Iran, in 1982. He received the PhD degree in microelectronics from Tyndall National Institute, University College Cork, Ireland, in 2011. Since 2012 he has been a researcher with the University of Western Australia, where he works on design of infra-red detectors and quantum transport in nanostructures.

Gilberto A. Umana-Membreno, received his PhD in Electrical and Electronic Engineering from the University of Western Australia (UWA) in 2007. His research interests are in the general area of semiconductor materials, micro- and nano-electronic/optoelectronic device characterization, design, optimisation and processing and fabrication.

Renjie Gu, received his Ph.D. in 2012 from Chinese Academy of Sciences, Shanghai, China. His current research is on MBE growth of HgCdTe materials.

Mohsen Asadnia, received his Ph.D. in 2014 from Singapore. He is working on GaN sensors for Hg detection in UWA.

Jarek Antoszewski, obtained his Ph.D. in 1982 from The Institute of Physics, Polish Academy of Science. From 2004, he involved in the UWA MEMS programs which resulted in demonstration of the first worldwide monolithically integrated micro-spectrometer based on combined MEMS and HgCdTe technologies.

Lorenzo Faraone (M'79-–SM'03–F'14) was born in Italy in 1951. He received the Ph.D. degree from the University of Western Australia (UWA), Crawley, WA, Australia, in 1979.

He has been at UWA since 1987. His current research interests include compound semiconductor materials and devices, and microelectromechanical systems.